Understanding the H2 sorption trends in the M-MOF-74 series (M = Mg, Ni, Co, Zn)

ARTICLE *in* THE JOURNAL OF PHYSICAL CHEMISTRY C · DECEMBER 2014

Impact Factor: 4.77 · DOI: 10.1021/jp510253m

6 AUTHORS, INCLUDING:

Tony Pham
University of South Florida
36 PUBLICATIONS **703** CITATIONS
SEE PROFILE

M. Gisela Orcajo
King Juan Carlos University
17 PUBLICATIONS **248** CITATIONS
SEE PROFILE

Brian Space
University of South Florida
91 PUBLICATIONS **1,960** CITATIONS
SEE PROFILE

THE JOURNAL OF PHYSICAL CHEMISTRY C

Article

pubs.acs.org/JPCC

Understanding the H_2 Sorption Trends in the M-MOF-74 Series (M = Mg, Ni, Co, Zn)

Tony Pham,[†] Katherine A. Forrest,[†] Rahul Banerjee,[‡] Gisela Orcajo,[∥] Juergen Eckert,[†] and Brian Space*[,†]

[†]Department of Chemistry, University of South Florida, 4202 East Fowler Avenue, CHE205, Tampa, Florida 33620-5250, United States

[‡]Physical/Materials Chemistry Division, CSIR-National Chemical Laboratory, Dr. Homi Bhabha Road, Pune 411008, India

[∥]Department of Chemical and Energy Technology, ESCET, Rey Juan Carlos University, C/Tulipán s/n, 28933 Móstoles, Madrid, Spain

Supporting Information

ABSTRACT: Electronic structure calculations and simulations of H_2 sorption were performed in four members of the M-MOF-74 series: Mg-MOF-74, Ni-MOF-74, Co-MOF-74, and Zn-MOF-74. Notable differences were observed in the partial charge and polarizability of the metal ions derived from the electronic structure calculations. The modeling parameters obtained from the electronic structure calculations were found to influence certain features in the experimentally observed H_2 sorption trends in the M-MOF-74 series. The simulations were performed with the inclusion of explicit many-body polarization, which was required to reproduce the experimental H_2 sorption observables (i.e., sorption isotherms and isosteric heats of adsorption (Q_{st})) and the H_2−metal interaction in all four MOFs using classical molecular simulation. Consistent with experimental measurements, the simulations captured the following trend for the H_2−metal interaction strength: Ni-MOF-74 > Co-MOF-74 > Mg-MOF-74 > Zn-MOF-74. The calculations revealed that stronger H_2−metal interactions within the M-MOF-74 series corresponded to shorter H_2−metal distances and higher induced dipoles on the metal-sorbed H_2 molecules. In addition, it was observed that there was a strong correlation between the H_2−metal interaction and the polarization contribution. Although Mg-MOF-74 has the highest calculated partial charge for the metal ion within the series, the Mg^{2+} ion has a very low polarizability compared to the other M^{2+} ions; this explains why the H_2−metal interaction in this MOF is weaker compared to those for Ni-MOF-74 and Co-MOF-74. The sterics interactions, reflected in the crystal structure for all four MOFs, also played a role for the observed H_2 sorption trends. Zn-MOF-74 has the lowest H_2 uptakes and Q_{st} within the series due to an unfavorable geometric environment for the Zn^{2+} ions within the ZnO_5 clusters. Lastly, the two-dimensional quantum rotational levels were calculated for the H_2−metal interaction in all four MOFs using the potential energy function employed herein and the calculated transitions were in good agreement with the corresponding peaks that were observed in the experimental inelastic neutron scattering (INS) spectra for the respective MOFs. This observation serves both to provide atomistic resolution to the spectroscopic experiments and to validate the molecular force field.

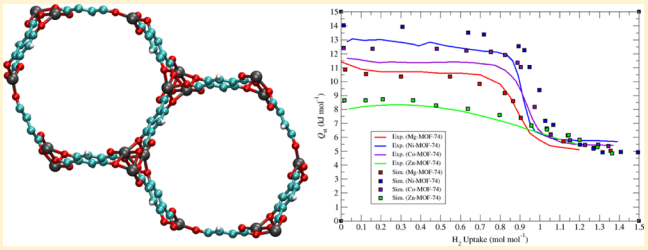

I. INTRODUCTION

Metal−organic frameworks (MOFs) are crystalline materials that have been shown to be one of the most promising candidates for applications in H_2 storage.[1−3] Consisting of metal ions coordinated to organic ligands, resulting in a porous three-dimensional structure, MOFs have the ability to effectively store H_2 molecules within the pores. They also have the ability to release the H_2 molecules freely through adjustments in thermodynamic conditions (e.g., decreasing the pressure or contact with a large reservior). Indeed, H_2 sorption in MOFs is characterized as physisorption, for which the typical interaction energy between the sorbate molecules and the material ranges from 5 to 50 kJ mol^{-1}. In addition, MOFs are highly tunable as a number of different structures can be synthesized or envisioned by substituting the metal ion and/or ligand. It is for these reasons that MOFs have advantages over competing materials, such as zeolites, activated carbons, and metal hydrides for H_2 storage applications. In order to use H_2 as a fuel source in vehicles, high H_2 uptake at room temperature and moderate pressures is required in a storage medium. In addition, a H_2 adsorption enthalpy within the range 15−30 kJ mol^{-1} has been proposed as desirable/aspirational for room temperature H_2 storage in porous materials.[4,5]

The M-MOF-74 series is one of the most popular classes of MOFs that exist in the MOF literature.[6−18] These MOFs are synthesized by combining M^{2+} ions with 2,5-dioxido-1,4-benzenedicarboxylate (dobdc) ligands. The resulting framework consists of a honeycomb-like structure with a pore diameter of nearly 12 Å (Figure 1). Different variants of this series of MOFs have been synthesized through changing the

Received: October 10, 2014
Revised: December 12, 2014
Published: December 12, 2014

DOI: 10.1021/jp510253m
J. Phys. Chem. C 2015, 119, 1078−1090

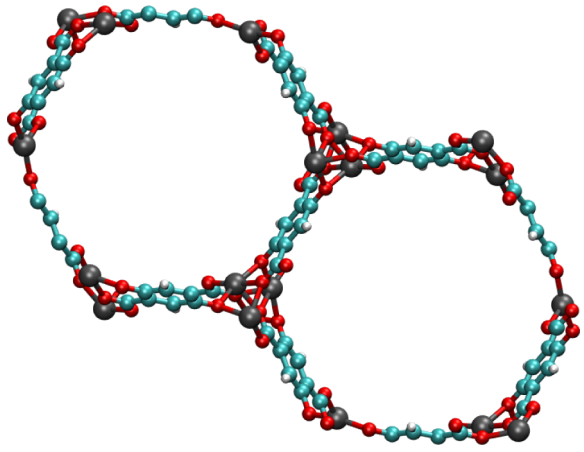

Figure 1. Orthographic *c* axis view of the 1 × 1 × 4 unit cell system of M-MOF-74. Atom colors: C = cyan, H = white, O = red, and Mg/Ni/Co/Zn = gray.

M^{2+} ion. Metal ions such as Mg^{2+}, Ni^{2+}, Co^{2+}, and Zn^{2+} have been used to construct a M-MOF-74 material. Each M^{2+} ion in the activated structure of these materials is connected to five oxygen atoms in a square pyramidal coordination environment. These metal centers are accessible through the cylindrical pores of the MOFs. Thus, each M^{2+} ion acts as an open-metal site, which is a highly favorable sorption site for various sorbate molecules, including H_2. Experimental H_2 sorption studies on several members of the M-MOF-74 series revealed that the H_2−metal interaction in these MOFs corresponds to a high initial isosteric heat of adsorption (Q_{st}) for H_2.[8,11,15,16,19,20] Indeed, initial H_2 Q_{st} values ranging from 8.0 to 13.5 kJ mol^{-1} have been reported through experimental measurements in the M-MOF-74 series. The Q_{st} values exhibited by some members of the M-MOF-74 series are close to the minimum target of 15 kJ mol^{-1} that is required for room temperature H_2 storage applications.

In this work, we parametrized and performed grand canonical Monte Carlo (GCMC) simulations of H_2 sorption in different members of the M-MOF-74 series. Specifically investigated herein for H_2 sorption were Mg-MOF-74, Ni-MOF-74, Co-MOF-74, and Zn-MOF-74; these are the most popular and widely studied members of the M-MOF-74 series. This was done in order to elucidate the H_2 sorption characteristics for each MOF. Although these MOFs are isostructural, they exhibit different experimental H_2 sorption properties, which is dependent on the identity of the metal. For instance, Ni-MOF-74 was shown to have an initial H_2 Q_{st} value ranging from 13.0 to 13.5 kJ mol^{-1} through experimental measurements,[11,15,19] while Zn-MOF-74 displayed an initial Q_{st} value in the range of 8.0 to 8.8 kJ mol^{-1}.[8,11,20] In this study, we attempt to understand the H_2 sorption trends within the M-MOF-74 series by first performing electronic structure calculations in each MOF to gain insights into the electrostatic and polarizable nature of the metal, and then executing subsequent GCMC simulations of H_2 sorption in the respective MOFs to see if we can reproduce the experimental measurements. It is expected that the metal partial charge and polarizability, in concert with the sterics of the crystal structure for each MOF, play a role for the observed H_2 sorption trends.

For the simulations in this work, it was necessary to include explicit many-body polarization effects to capture the H_2−metal interactions in these MOFs via GCMC simulation. Note, although the interaction between the sorbate molecules and the metals in this class of MOFs can be captured in simulation using other methods (e.g., *ab initio* force fields, density functional theory),[11,21−26] classical polarization is currently the only way to achieve this in a classical simulation that has very desirable system size scaling and associated relatively low computational cost. We have shown in previous work that the inclusion of cooperative polarization was requisite and effective in capturing the sorption of H_2 molecules onto the accessible Cu^{2+} ions of copper paddlewheel, $[Cu_2(O_2CR)_4]$, clusters in classical molecular simulation in MOFs that contain these units.[27−30] It will be demonstrated in this work that such interactions were also efficacious for the accurate simulations of H_2 sorption in these MOFs that contain open-metal sites through the MO_5 units. Indeed, it is shown here that the simulated H_2 sorption isotherms and associated Q_{st} values in each MOF are in quite good agreement with the corresponding experimental data when polarization is included.

Furthermore, slight differences can be observed in the experimental inelastic neutron scattering (INS) spectra for H_2 in the four M-MOF-74 analogues. Nonetheless, the INS spectra for Mg-MOF-74, Ni-MOF-74, Co-MOF-74, and Zn-MOF-74 revealed rotational tunnelling transitions that occur at similar energies.[15,20,31] This makes reproducing this spectroscopic observable a challenge for our mechanical energy function. Further, unlike the trends in the initial H_2 Q_{st} values (and therefore, the H_2−metal interactions), no apparent trends can be observed when comparing the features in the INS spectra between the four MOFs. From this data, it is predicted that the rotational potential for the H_2−metal interaction in these MOFs is nearly independent of the identity of the metal. This phenomenon will be investigated and confirmed through two-dimensional quantum rotation calculations for the H_2−metal interaction in the respective MOFs. These calculations were performed using the analytical potential energy function employed in this work. Note, we have successfully calculated the rotational transitions for various H_2 sorption sites in different MOFs in previous work using this method.[29,30,32−34]

II. METHODS

Simulations of H_2 sorption were performed in all considered M-MOF-74 variants in the 1 × 1 × 4 unit cell system of the respective MOFs as shown in Figure 1. The simulations were executed using GCMC methods,[35] which is described in detail in the Supporting Information. The potential energy of the MOF−H_2 system was calculated through the sum of the repulsion/dispersion energy, electrostatic energy, and many-body polarization energy. These were computed through the use of the Lennard-Jones 12−6 potential, Ewald summation,[36] and a Thole−Applequist type model,[37−40] respectively. For the simulations of H_2 sorption at the temperatures considered in this work, quantum mechanical dispersion effects were included semiclassically through Feynman−Hibbs corrections to the fourth order.[41] Note, it was necessary to include the polarization term to the potential energy function for the simulations of H_2 sorption in these MOFs. The inclusion of polarization was required to reproduce the experimental isotherms at low loading and Q_{st} values in the respective MOFs. Correspondingly, the induction term was required to capture the sorption of H_2 onto the open-metal sites in classical GCMC simulation. More details of the polarization model used in this work can be found in the Supporting Information. All H_2 sorption simulations performed in this work utilized an accurate

DOI: 10.1021/jp510253m
J. Phys. Chem. C 2015, 119, 1078−1090

and transferable five−site polarizable potential that was developed previously.[42]

Mg-MOF-74 was parametrized in previous work by our group[43] and the resulting parameters are used herein. Ni-MOF-74, Co-MOF-74, and Zn-MOF-74 were parametrized in an analogous manner as Mg-MOF-74. Note, none of the MOF or sorbate parameters in this manuscript were adjusted or selected to facilitate agreement with the experimental isotherms and Q_{st} data for H_2 sorption in these MOFs. For each MOF, the Lennard-Jones parameters for all MOF atoms were taken from the universal force field (UFF).[44] It is important to mention that using parameters from known general purpose force fields like the UFF is not ideal for calculating van der Waals interactions between the MOF and the sorbate molecules. However, as explained above, our potential energy function consists of three terms that describe the total energy of the MOF−H_2 system. As observed in our previous work on Mg-MOF-74[43] and shown herein, H_2 sorption in the majority of members in the M-MOF-74 series is dominated by polarization interactions. Thus, while the choice of van der Waals parameters is possibly nonoptimal, there is little known sensitivity to a reasonable choice as far as the relative importance of polarization in understanding the H_2−metal interactions. In addition, such parameters have been shown to be remarkably effective over a wide variety of state points.[45]

The partial charges for the chemically distinct atoms in each MOF were determined through electronic structure calculations on a series of gas phase fragments that were based on the crystal structure of the respective MOFs. There are a total of 9 atoms in chemically distinct environments in the M-MOF-74 system (Figure 2). For Ni-MOF-74, Co-MOF-74, and Zn-MOF-74, fragments of similar type to those selected for Mg-MOF-74[43] were chosen for the electronic structure calculations. The calculated partial charges for the chemically distinct atoms in all four MOFs can be found in Table 1. These charges were used in the simulations in this work to calculate the electrostatic energy of the MOF−H_2 system. While the partial charges for most distinguishable atoms are very similar between the four MOFs, there are noticeable differences in the charges of the metal ions between the MOFs. Electronic structure calculations on the different M-MOF-74 analogues revealed the following trend for the calculated partial charges for the M^{2+} ions: Mg^{2+} > Ni^{2+} > Zn^{2+} > Co^{2+}.

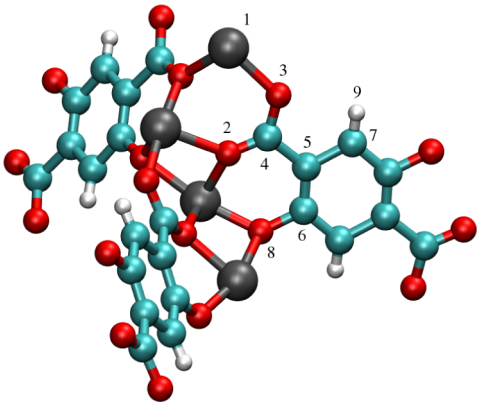

Figure 2. Numbering of the chemically distinct atoms in M-MOF-74 as referred to in Table 1. Atom colors: C = cyan, H = white, O = red, and Mg/Ni/Co/Zn = gray.

Table 1. Calculated Partial Charges (e^-) for the Chemically Distinct Atoms in the M-MOF-74 Series (M = Mg, Ni, Co, Zn)[a]

atom	label	Mg-MOF-74	Ni-MOF-74	Co-MOF-74	Zn-MOF-74
M	1	1.678 00	1.501 50	1.420 10	1.492 40
O	2	−0.871 40	−0.780 00	−0.794 50	−0.829 60
O	3	−0.768 00	−0.664 70	−0.589 40	−0.757 10
C	4	0.930 30	0.882 60	0.939 40	0.879 80
C	5	−0.481 50	−0.449 10	−0.527 00	−0.267 50
C	6	0.467 50	0.440 70	0.490 00	0.404 20
C	7	−0.382 40	−0.439 10	−0.403 20	−0.374 10
O	8	−0.805 40	−0.716 50	−0.729 10	−0.774 20
H	9	0.232 90	0.224 60	0.193 70	0.226 10

[a]Labeling of atoms corresponds to Figure 2.

Atomic point polarizabilites were assigned to the nuclear center of all atoms of the framework for each MOF in order to model explicit many-body polarization. The polarizabilities for all C, H, and O atoms were taken from a rigorously parametrized set[46] that was shown to be highly transferable.[27−30,47−49] Thus, these atoms were assigned the exponential damping type polarizabilities (C = 1.28860 Å^3, H = 0.41380 Å^3, O = 0.85200 Å^3) and associated damping parameter provided by the work of van Duijnen and Swart.[46] The polarizability parameter for Mg^{2+}, Ni^{2+}, Co^{2+}, and Zn^{2+} were not included in the aforementioned set, and thus, they were determined using *ab initio* methods as explained below. Note, while the model employs scalar point polarizability parameters, the interaction between them results in site tensors.

For each M^{2+} ion, the polarizability tensor for small fragments (e.g., MO, MX_2) containing that ion was calculated using the Q-Chem code[50] with the aug-cc-pVDZ basis applied to all atoms. The parameter for the M^{2+} ion was then optimized such that a derived molecular polarizability tensor, calculated using the aforementioned Thole−Applequist type model, was in close agreement to the tensor that was produced from the quantum mechanical calculations. This derived molecular polarizability tensor was calculated using the Massively Parallel Monte Carlo (MPMC) code,[51] an open-source code that is available for download on Google Code. The average calculated values for the polarizability of the M^{2+} ions are provided in Table 2. These values were used for the polarizability of the M^{2+} ions in the simulations in this work. The following trend can be observed for the calculated polarizabilities for the different M^{2+} ions: Co^{2+} > Ni^{2+} > Zn^{2+} > Mg^{2+}. The trend in the polarizabilities for the transition metals is consistent with the atomic/ionic radius trend for the periodic table. Typically, the polarizability increases with increasing volume of the atom.

Table 2. Calculated Polarizabilities (Å^3) for the Different M^{2+} Ions

M^{2+} ion	$\alpha°$ (Å^3)
Mg^{2+}	0.007 20
Ni^{2+}	2.946 50
Co^{2+}	3.264 40
Zn^{2+}	1.988 70

The rotational energy levels for a H_2 molecule sorbed about the M^{2+} ion in each MOF were also calculated and compared to the rotational tunnelling transitions that are observed in the INS spectra for the respective MOFs. An optimized position for

DOI: 10.1021/jp510253m
J. Phys. Chem. C 2015, 119, 1078−1090

a H_2 molecule sorbed in proximity to the metal ion in each MOF was obtained in simulation using simulated annealing.[52] These rotational levels were calculated by solving the two-dimensional rigid-rotor Hamiltonian for the H_2−metal interaction in each MOF using methods described previously.[29,30,32−34] The potential energy surface for the H_2 molecule rotating in the vicinity of the metal ion in the MOF was calculated using the analytical potential energy function utilized in this work. All calculations were performed in the 1 × 1 × 4 system cell of the respective MOFs. More details of performing the two-dimensional quantum rotation calculations can be found in the Supporting Information.

III. RESULTS AND DISCUSSION

A. Isotherms and Isosteric Heats of Adsorption. The experimental and simulated H_2 sorption isotherms for pressures up to 100 kPa in all four M-MOF-74 variants at 77 and 87 K are shown in Figure 3a and 3b, respectively. All experimental data shown in this work for Mg-MOF-74, Ni-MOF-74, and Co-MOF-74 were extracted and/or estimated from ref 15. This study reports the highest H_2 uptakes and Q_{st} values for these MOFs through experimental measurements, suggesting that the MOF samples that were used in that work were perhaps better activated. Indeed, according to the experiments performed in ref 15, the samples for all three MOFs were extensively and perhaps fully activated prior to H_2 sorption measurements. Note, the experimental data for Zn-MOF-74 was estimated from ref 8, since ref 15 did not perform measurements for this MOF.

It can be observed that the experimental H_2 sorption isotherms for Mg-MOF-74, Ni-MOF-74, and Co-MOF-74 at both temperatures exhibit an initial steep increase in uptake for pressures below 5 kPa. As the pressure increases, Mg-MOF-74 gets higher H_2 uptake within the series for the remainder of the low-pressure regime (up to 100 kPa). Ni-MOF-74 sorbs the next highest amount of H_2, followed by Co-MOF-74. Zn-MOF-74 sorbs the lowest quantity of H_2 at all pressures for both temperatures. The simulations performed in this work were able to closely replicate the experimental isotherms for all four MOFs. Indeed, all considered simulation points for each MOF are in very good agreement with the corresponding experimental data to within joint uncertainties at both temperatures.

Note, physically reasonable simulated isotherms like those shown in Figure 3a and 3b, for all four M-MOF-74 analogues can only be produced using a polarizable H_2 model as employed in this work in classical GCMC simulation. Models that neglect explicit induction are not sufficient to reproduce the experimental isotherms in these MOFs due to the highly charged and polarizable environment of these frameworks. For instance, simulations using the single−site Lennard-Jones potential by Buch,[53] the five−site nonpolarizable potential by Belof et al.,[42] and the well-known three−site charge-quadrupole model by Darkrim and Levesque[54] in all four MOFs failed to reproduce the experimental H_2 sorption isotherms in the respective MOFs, as the isotherms that were generated by these models undersorbed the corresponding experimental data by a significant amount (see Supporting Information). Perhaps what is surprising is the reliability of using classical many-body polarization to capture the metal−sorbate interactions quantitatively; this is a theme that has now been well-documented.[27−30,55,56]

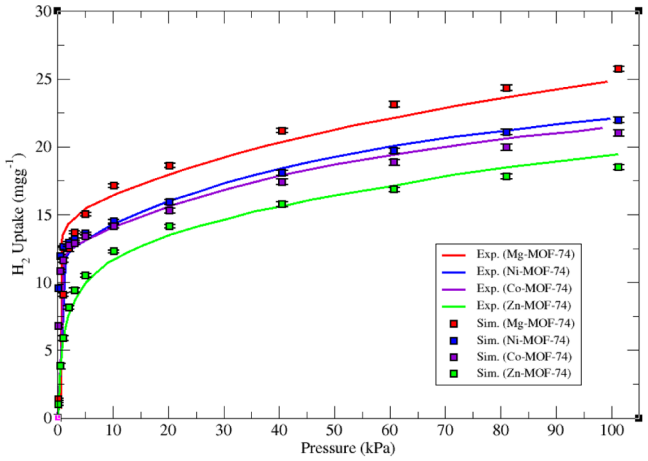

(a)

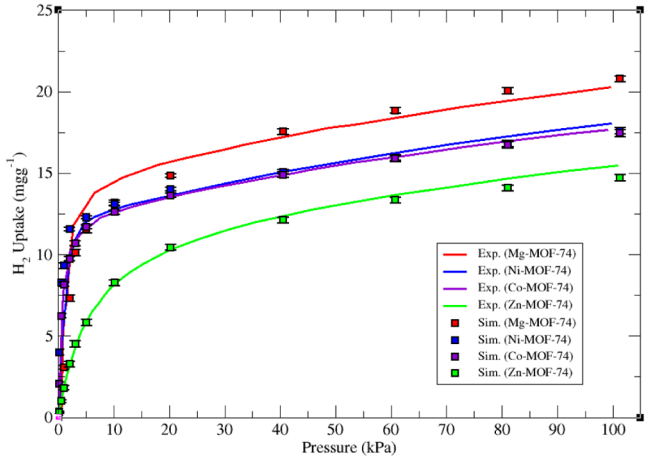

(b)

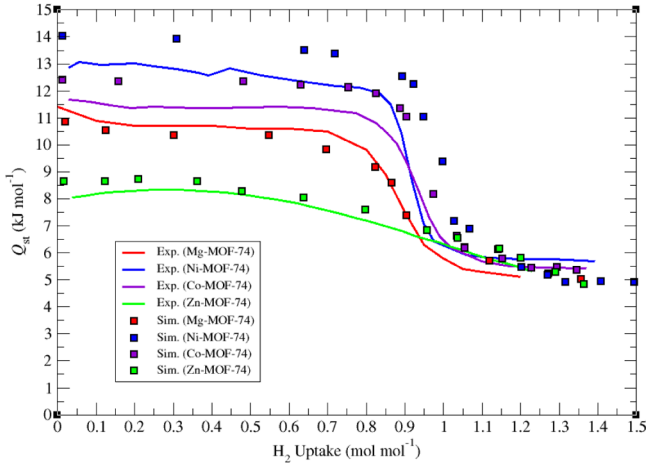

(c)

Figure 3. Low-pressure (up to 100 kPa) absolute H_2 sorption isotherms in Mg-MOF-74 (red), Ni-MOF-74 (blue), Co-MOF-74 (violet), and Zn-MOF-74 (green) at (a) 77 K and (b) 87 K for experiment (solid lines) and simulation (squares). (c) Isosteric heats of adsorption, Q_{st}, for H_2 plotted against hydrogen uptakes. The experimental data for Mg-MOF-74, Ni-MOF-74, and Co-MOF-74 were taken from ref 15 (reproduced with permission within the guidelines provided by the Royal Society of Chemistry. Copyright 2010 Royal Society of Chemistry), while those for Zn-MOF-74 were taken from ref 8 (reproduced within the guidelines provided by the American Chemical Society. Copyright 2006 American Chemical Society).

DOI: 10.1021/jp510253m
J. Phys. Chem. C 2015, 119, 1078−1090

The GCMC-calculated Q_{st} values for H_2 in all considered M-MOF-74 variants are shown in Figure 3c and compared to the corresponding experimental values for each MOF. Experimental studies show the following trend for the initial H_2 Q_{st} values within the M-MOF-74 series: Ni-MOF-74 > Co-MOF-74 > Mg-MOF-74 > Zn-MOF-74. The unit of loading reported in Figure 3c is moles of H_2 per moles of MOF; this is equivalent to the number of H_2 molecules per metal ion. As shown in the figure, the aforementioned experimental trend is surprisingly reproduced from the simulations in this work. The simulated Q_{st} values in each MOF are in good agreement with the corresponding experimental results for each MOF for the loading range considered. Note, the Q_{st} values that are shown in Figure 3c are a quantity estimated from the isotherms experimentally, but such values are obtained directly from GCMC simulations. Thus, directly comparing isotherms between experiment and simulation can be a better metric than comparing the Q_{st} values in cases where the finite difference procedure, inherent in the experimental data analysis, is difficult (e.g., when the isotherm curves are nearly parallel).

Ni-MOF-74 exhibits the highest initial H_2 Q_{st} value within the series, with a value of approximately 13.0 kJ mol^{-1}. This is in very good agreement to what was calculated for H_2 sorption in Ni-MOF-74 through infrared (IR) spectroscopy (13.5 kJ mol^{-1}).[19] The simulations predict that the initial Q_{st} value is 14.0 kJ mol^{-1}, which is in the vicinity of the aforementioned values. Co-MOF-74 has the next highest initial H_2 Q_{st} (11.9 kJ mol^{-1}), followed by Mg-MOF-74 (11.4 kJ mol^{-1}). The simulations predict initial Q_{st} values of 12.4 and 10.8 kJ mol^{-1} for Co-MOF-74 and Mg-MOF-74, respectively, which are close to the corresponding experimental values. The very high initial Q_{st} values for Mg-MOF-74, Ni-MOF-74, and Co-MOF-74 indicate strong physisorptive interactions between the H_2 molecules and the M^{2+} ions in the respective MOFs. For these three M-MOF-74 variants, the experimental Q_{st} values are nearly constant for all loadings up to about 0.80 mol mol^{-1}. Afterward, the Q_{st} values for these MOFs sharply decrease, as they fall to a value of about 5.5 kJ mol^{-1} at 1.0 mol mol^{-1} loading. This implies that all metal sites for each MOF are fully occupied at a loading of roughly 1.0 mol mol^{-1}. At loadings beyond 1.0 mol mol^{-1}, the Q_{st} values are relatively constant at around 5.5 kJ mol^{-1} for the three MOFs; this value is associated with sorption onto the secondary sites. The shapes and magnitudes of the experimental Q_{st} plot for these three MOFs have been closely reproduced by the simulations in this work.

Even though Mg-MOF-74 has higher H_2 uptake for most of the considered low-pressure region at both temperatures compared to Ni-MOF-74 and Co-MOF-74, the initial Q_{st} values for Mg-MOF-74 are still lower than those for the Ni and Co analogues. In terms of empirical fitting, the experimental Q_{st} values for H_2 are higher for Ni-MOF-74 and Co-MOF-74 because the 77 and 87 K sorption isotherms for the respective MOFs are close to each other in uptakes and shape. On the other hand, the experimental isotherms for the two temperatures for Mg-MOF-74 are more spread out from each other, thus explaining the lower H_2 Q_{st} for this MOF from an empirical fitting point of view. It can be observed that the simulated uptakes at both temperatures rise more sharply at pressures below 5 kPa for Ni-MOF-74 and Co-MOF-74 compared to Mg-MOF-74 (Figure 3a and 3b). This is consistent with the trends in the simulated Q_{st} values at low loading (Figure 3c), as a sharper increase in loading within this region usually corresponds to a higher Q_{st}. However, as observed in experiment and simulation, Mg-MOF-74 sorbs a higher quantity of H_2 for the remainder of the pressure range considered. This suggests that the secondary sorption sites are more favorable in Mg-MOF-74 than in the other two variants.

Consistent with the trends in the H_2 uptakes, the Q_{st} values for Zn-MOF-74 are the lowest within the series. The experimental Q_{st} value for this MOF starts at around 8.0 kJ mol^{-1} and it remains roughly constant until a loading of about 0.70 mol mol^{-1}. Note, the aforementioned initial H_2 Q_{st} value for Zn-MOF-74 is close to what was reported for this MOF in previous work.[11,20] Afterward, the experimental Q_{st} plot begins to decrease in slope and it declines to values that are in the vicinity to those for the other three M-MOF-74 analogues as observed at loadings of 1.0 mol mol^{-1} and beyond. Unlike the experimental Q_{st} plot for the other three M-MOF-74 variants, the plot for Zn-MOF-74 does not exhibit the noticeable sharp decrease via the inverse sigmoidal shape. This suggests that the energetics for sorption onto the metals and the secondary sites in Zn-MOF-74 are relatively close to each other, which is in contrast to what was observed for the other three analogues. The simulations performed in this work for Zn-MOF-74 resulted in Q_{st} values that are in good agreement with experiment for all loadings considered. The shape in the experimental Q_{st} plot for Zn-MOF-74 was also reproduced in simulation. An initial H_2 Q_{st} value of 8.7 kJ mol^{-1} was calculated for Zn-MOF-74 for the simulations in this work, which is close to the corresponding experimental value.

As with the simulated H_2 uptakes, the GCMC-calculated Q_{st} values shown in Figure 3c for all four MOFs can only be produced using a polarizable potential for the MOFs and the sorbate in classical molecular simulation. Simulations of H_2 sorption using the previously described nonpolarizable potentials in these MOFs did not generate Q_{st} values that were representative of experiment in both magnitudes and shape for the respective MOFs (see Supporting Information). Note, the observed experimental and simulated H_2 Q_{st} trend for the M-MOF-74 series in this work is consistent with what was reported for this series in previous work using density functional theory (DFT) methods, with similar Q_{st} values being obtained.[11]

B. H_2–Metal Distances. Next, simulated annealing calculations[52] were employed using our polarizable force field for a single H_2 molecule in each MOF. This was done in order to obtain an optimal (energy mininum) position for the sorbate molecule about the metal ions within the respective frameworks. The calculations revealed noticeable differences for the optimized positions between the center-of-mass (COM) of the sorbed H_2 molecule and the M^{2+} ion in each MOF; the results are summarized in Table 3. Molecular illustrations depicting the H_2–metal interaction in each MOF as determined through minimization are shown in Figure 4. Notable differences can also be observed for the overall geometry of the sorbed H_2 molecules about the M^{2+} ions in all four MOFs (Figure 4); this resulted in differences in the distances between the H atoms of the H_2 molecule and the surrounding oxygen atoms (Table 3).

According to our calculations, the H_2 molecule sorbs closest to the metal in Ni-MOF-74, with a Ni^{2+}–COM distance of about 2.34 Å. Co-MOF-74 has the next shortest H_2–metal interaction distance, followed by Mg-MOF-74 and then Zn-MOF-74. It can observed that that the lower the M^{2+}–COM distance, the higher the initial H_2 Q_{st}. This makes sense given the interaction energy is expected to be greater as the H_2–metal distance decreases. Thus, there is a strong correlation

DOI: 10.1021/jp510253m
J. Phys. Chem. C 2015, 119, 1078–1090

Table 3. Observed Distances (Å) between Various Atoms of the M^{2+}−H_2 Interaction in the M-MOF-74 Series (M = Mg, Ni, Co, Zn)[a]

atom pair	Mg-MOF-74	Ni-MOF-74	Co-MOF-74	Zn-MOF-74
M^{2+}−COM	2.550 07	2.341 79	2.452 67	2.678 25
O1−H1	3.372 28	2.948 37	3.523 45	3.703 22
O2−H1	3.028 88	2.757 45	3.109 04	3.066 90
O3−H1	3.589 44	3.275 74	3.416 98	3.450 45
O4−H1	3.283 39	2.995 35	2.797 99	3.552 58
O1−H2	3.413 60	3.406 12	3.440 41	3.457 61
O2−H2	3.524 46	3.170 17	3.483 39	3.217 25
O3−H2	3.186 99	2.999 80	2.887 29	2.749 18
O4−H2	3.340 33	2.780 75	2.759 06	3.293 52

[a]Labeling of atoms corresponds to Figure 4. COM refers to the center-of-mass of the sorbed H_2 molecule. The positions of the H_2 molecules were determined through simulated annealing using our polarizable force field.

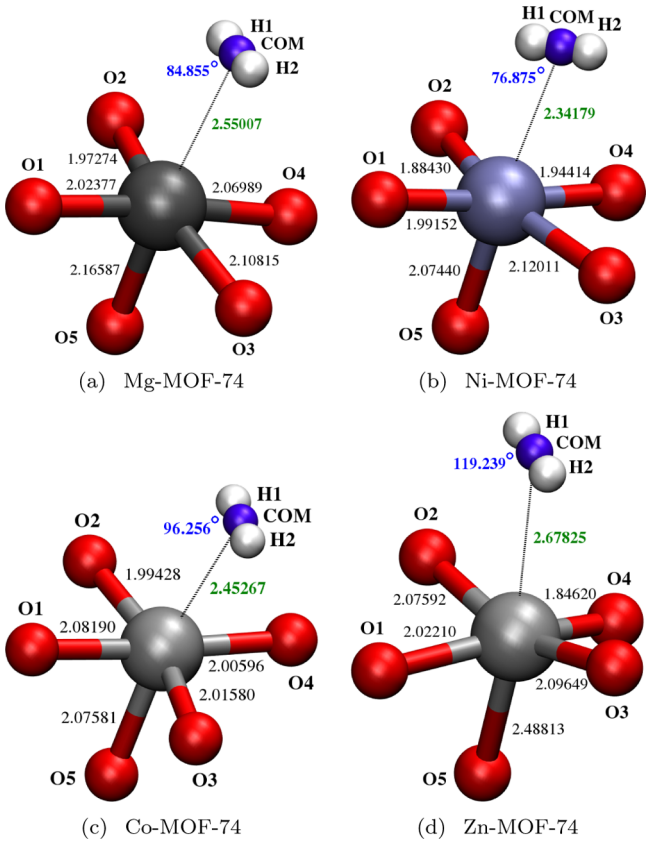

Figure 4. Molecular illustration of a sorbed H_2 molecule onto the M^{2+} ion in (a) Mg-MOF-74, (b) Ni-MOF-74, (a) Co-MOF-74, and (d) Zn-MOF-74 as determined from simulated annealing. The distances (Å) between the center-of-mass (COM) of the sorbed H_2 molecule and the M^{2+} ion are shown in green for all four MOFs, while the M^{2+}−COM−H1 angles (deg) are shown in blue. The distances (Å) between the M^{2+} ion and the surrounding oxygen atoms based on crystallography are also shown for each MOF. Atom colors: H = white, O = red, Mg = gray, Ni = lavender, and Co/Zn = silver. Note, the COM of the sorbed H_2 molecule is shown in violet.

between the H_2−metal distance and the Q_{st} values in these MOFs. Note, the M^{2+}−COM distances reported in Table 3 can only be obtained using a polarizable H_2 potential when classical molecular simulation is considered. Simulations using the previously described nonpolarizable H_2 potentials in each MOF captured much longer H_2−metal distances (>3.0 Å).

The M^{2+}−COM distance that was calculated for Mg-MOF-74 in this work (2.55 Å) is in very good agreement to what was calculated for the H_2−metal interaction in this MOF through DFT calculations in previous work (2.54 Å).[11] Further, this distance is comparable to the corresponding distance that was obtained in Mg-MOF-74 through neutron powder diffraction (NPD) studies (2.45 Å).[16] In our previous work on H_2 sorption in Mg-MOF-74, we observed that the majority of H_2 molecules sorbed onto the Mg^{2+} ions with a H_2−metal distance of 2.60 Å with our polarizable potential in GCMC simulation.[43] We observed in this work that the H_2 molecule can get a little closer to the metal in Mg-MOF-74 using simulated annealing to obtain minimum energy geometries.

For Zn-MOF-74, our calculations revealed a M^{2+}−COM distance of approximately 2.68 Å; this is in good agreement to the corresponding distance based on NPD studies in Zn-MOF-74 (ca. 2.60 Å).[20] Our calculated distance for the H_2−metal interaction in Zn-MOF-74 is notably shorter than what was calculated in this MOF in the aforementioned DFT studies (2.83 Å).[11] Note, the same DFT studies revealed M^{2+}−COM distances in Ni-MOF-74 and Co-MOF-74 that are significantly shorter than what was calculated in this work for the respective MOFs, with distances of 2.00 and 2.13 Å for Ni-MOF-74 and Co-MOF-74, respectively.[11] While H_2−metal distances near 2.0 Å are close to what have been observed for coordinated dihydrogen (<1.9 Å),[57,58] for which there is no evidence in these MOFs, the trend in the M^{2+}−COM distances given in ref 11 are consistent with our results. NPD studies in Ni-MOF-74 and Co-MOF-74 revealed M^{2+}−COM distances of 2.20 and 2.32 Å, respectively.[59,60] These distances are closer to the values that were obtained in this work through simulated annealing calculations using our polarizable force field than those obtained in the aforementioned DFT studies for the respective MOFs. Note, even though the results from the polarizable H_2 potential are reported in this work, the electrostatic potentials were able to capture the same relative trend in the M-MOF-74 series despite much longer H_2−metal distances, likely because stronger electrostatic interactions also imply larger polarization. Steric effects within the crystal structures of the MOFs should also play a role in this.

C. Dipole Distributions. In order to gain further insights into the relative energetics for the H_2−metal interaction in all four M-MOF-74 variants, we examined the distribution of induced dipoles resulting from the polarizable H_2 potential in the respective MOFs. The normalized dipole distribution for all four MOFs at 77 K and 0.20 atm are shown in Figure 5. This graph plots the normalized sorbate population as a function of the induced dipole magnitudes for each sorbed H_2 molecule in the MOF. While the dipole moment of a single H_2 molecule averages 0 D in bulk, our simulations in the M-MOF-74 series show that the external field of the MOF causes the majority of the sorbed H_2 molecules to exhibit a dipole moment. Thus, the sorbed H_2 molecules are characteristic of a dipolar fluid. The resulting figure shows a number of distinct peaks, with each peak corresponding to a particular site or region of occupancy inside the MOF.

As explained in our previous work on Mg-MOF-74,[43] the high dipole magnitude peak (i.e., the peak on the far right for the respective M-MOF-74 analogues) corresponds to the sorption of H_2 onto the metal centers in this series of MOFs. Since the M^{2+} ions in each MOF are highly charged/polar,

DOI: 10.1021/jp510253m
J. Phys. Chem. C 2015, 119, 1078−1090

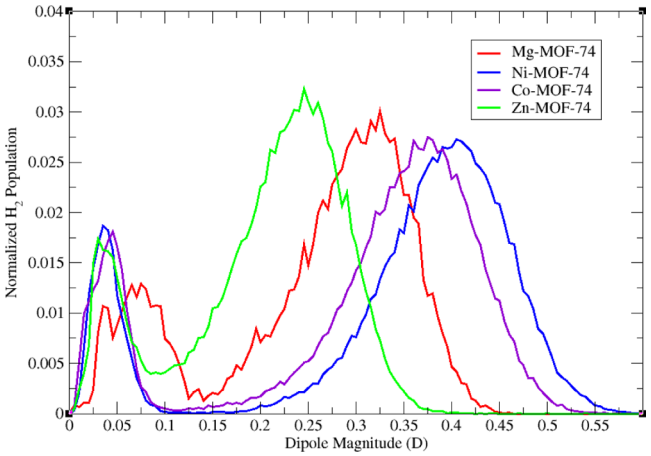

Figure 5. Normalized H_2 dipole distribution at 77 K and 0.20 atm in Mg-MOF-74 (red), Ni-MOF-74 (blue), Co-MOF-74 (violet), and Zn-MOF-74 (green).

these sites would induce significantly high dipoles on the H_2. Notable differences can be observed for the dipole magnitudes corresponding to sorption onto the M^{2+} ions between the four MOFs. As shown in Figure 5, the Ni^{2+} ions in Ni-MOF-74 induces the highest dipoles on the sorbed H_2 molecules within the series, with dipole magnitudes in the range of 0.25 to 0.55 D. The high dipole magnitude peak for Co-MOF-74 is slightly shifted to the left as this peak spans from 0.225 to 0.50 D. This indicates slightly weaker H_2–metal interaction in Co-MOF-74 compared to Ni-MOF-74. For Mg-MOF-74, the high dipole magnitude peak ranges from 0.175 to 0.425 D, thus indicating that the H_2–metal interaction in this MOF is weaker than those for Ni-MOF-74 and Co-MOF-74. The Zn^{2+} ions induces the lowest dipoles on the sorbed H_2 molecules within the series, with dipole magnitudes ranging from 0.10 to 0.35 D. The trends for the induced dipole magnitudes for the H_2–metal interaction in this series of MOFs are consistent with the trends in the initial H_2 Q_{st} values—that is, Ni-MOF-74 > Co-MOF-74 > Mg-MOF-74 > Zn-MOF-74.

For Ni-MOF-74, Co-MOF-74, and Zn-MOF-74, the low dipole magnitude peak can be observed from 0.00 to 0.10 D for these three MOFs. For Mg-MOF-74, this peak is slightly shifted to the right as this peak spans from 0.025 to 0.125 D. This low dipole magnitude peak corresponds to H_2 molecules sorbed at the secondary sites in these MOFs. NPD studies in certain members of this series of MOFs revealed that the secondary sorption sites are in the vicinity of the oxygen atoms (e.g., the oxido groups of the linkers).[16,20] This is consistent to what was observed for the secondary sorption sites in Mg-MOF-74 in our previous computational work.[43] The same sorption sites can be observed for the other three M-MOF-74 variants. Indeed, after the metal sites are filled, the H_2 molecules sorb in the proximity of the neighboring metal–coordinated oxygen atoms in these MOFs. As observed in the experimental and simulated Q_{st} plots for the four MOFs, the H_2 binding energy associated with the secondary site is approximately 5.5 kJ mol^{-1}.

The fact that the low dipole magnitude peak for Mg-MOF-74 has slightly higher dipoles than those for Ni-MOF-74, Co-MOF-74, and Zn-MOF-74 suggests that the secondary sorption sites are more favorable in this MOF compared to the other three variants. This is likely because the oxygen atoms are more negatively charged in Mg-MOF-74 than the other three analogues (Table 1), which allows for stronger interactions between the H_2 molecules and the framework O atoms. These oxygen atoms are more negatively charged in Mg-MOF-74 because the Mg^{2+} ions are highly electropositive. This could be the reason for why Mg-MOF-74 sorbs a higher quantity of H_2 than the other M-MOF-74 variants for most of the considered low-pressure range at both 77 and 87 K.

Note, it can be observed that the high dipole magnitude peak for Zn-MOF-74 is slightly higher in intensity compared to those for the other three MOFs for the state point considered. This is because there are more relative H_2 molecules sorbing onto the metals in Zn-MOF-74 at 77 K and 0.20 atm than in the other three M-MOF-74 analogues. For Mg-MOF-74, Ni-MOF-74, and Co-MOF-74, there is a greater number of H_2 molecules sorbing onto the metal ions in these MOFs at lower pressures.

Although the normalized H_2 dipole distribution for the four MOFs at 77 K and 0.20 atm are shown here in the main text, similar distributions can be observed for the respective MOFs at other pressures, but the intensities of the peaks vary depending on the pressure. For all MOFs, the high dipole magnitude peak increases in intensity at lower pressures and decreases in intensity at higher pressures, while the opposite effect can be observed for the low dipole magnitide peak. The normalized dipole distribution for H_2 at 77 K and various pressures from 0.001 to 1.0 atm for all four MOFs can be found in the Supporting Information.

D. Polarization Contributions and Energies. In order to assess the importance of polarization for simulations of H_2 sorption in the M-MOF-74 series, we examined the percent contributions and absolute magnitudes of the polarization energy in all four MOFs. The polarization contributions and energies are plotted at 77 K and pressures up to 1.0 atm for each MOF in Figure 6. It can observed that polarization

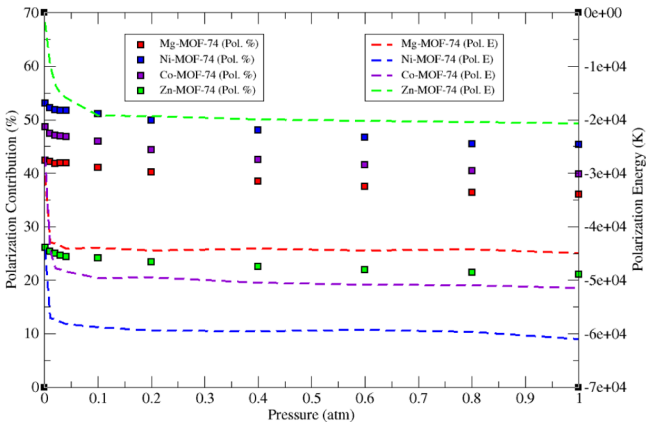

Figure 6. Percent contributions of the polarization energy (squares) for H_2 sorption in Mg-MOF-74 (red), Ni-MOF-74 (blue), Co-MOF-74 (violet), and Zn-MOF-74 (green) at 77 K and pressures up to 1.0 atm. The absolute magnitudes of the polarization energy (in K) are depicted as dashed lines on the opposite *y*-axis.

contributes to approximately 53% of the total energy for H_2 sorption in Ni-MOF-74 at initial loading. This is the highest percentage from polarization under this condition within the M-MOF-74 series. Note, the rest of the contributions is attributed to van der Waals and electrostatic interactions. For Ni-MOF-74, the polarization contribution slightly decreases as the pressure increases and reaches a percentage of about 45% at 1.0 atm.

DOI: 10.1021/jp510253m
J. Phys. Chem. C 2015, 119, 1078–1090

At initial loading, the contributions from polarization for H_2 sorption in Co-MOF-74 and Mg-MOF-74 are approximately 49% and 42%, respectively; these values mildly decrease to approximately 40% and 36% at 1.0 atm for the respective MOFs. Although these percentages are not as high as those for Ni-MOF-74, they are still substantial and demonstrates the importance of polarization in these two MOFs. For Mg-MOF-74, Ni-MOF-74, and Co-MOF-74, polarization is the main contributor to the total energy for H_2 sorption in these MOFs for the entire pressure range considered. Compared to the other M-MOF-74 variants, polarization does not contribute significantly to the sorption structure for H_2 in Zn-MOF-74. Indeed, polarization contributes to about 26% of the total energy initially for H_2 sorption in this MOF and it decreases to roughly 21% at 1.0 atm. This suggests that H_2 sorption in Zn-MOF-74 is more dominated by van der Waals and electrostatic interactions (further decomposition of the total energy indicates the former). Note, even though polarization does not contribute to a significant portion of the total energy in Zn-MOF-74, the inclusion of explicit polarization was still required to reproduce the experimental H_2 sorption observables in this MOF.

The absolute magnitudes of the polarization energy follow a similar trend to that for the polarization contribution for all four MOFs. The polarization energy for H_2 sorption in Ni-MOF-74 is the greatest (more negative) at all loadings within the series. Indeed, the polarization energy for Ni-MOF-74 reaches a value of nearly -6.1×10^4 K at 1.0 atm. Co-MOF-74 has the second highest polarization energy for all pressures, followed by Mg-MOF-74. Zn-MOF-74 has the lowest polarization energy for H_2 sorption at all pressures within the series, as the polarization energy starts at about -1.8×10^3 K at initial loading and only climbs to a value of nearly -2.1×10^4 K at 1.0 atm. Overall, the following trend can be observed within the polarization contribution and energy for H_2 sorption in the M-MOF-74 series: Ni-MOF-74 > Co-MOF-74 > Mg-MOF-74 > Zn-MOF-74. This is indeed consistent with the trends in the H_2−metal interaction as described above. This suggests that there is a high correlation between the observed H_2 sorption trends and the contributions from polarization within the M-MOF-74 series.

Note, although the metals are highly charged in these M-MOF-74 variants, stationary electrostatic interactions do not contribute as much to the total energy as polarization for H_2 sorption in Mg-MOF-74, Ni-MOF-74, and Co-MOF-74. The high metal charges greatly influence the contributions of electronic polarization in these MOFs when such effects are included in simulation. The percentages from electrostatic interactions for H_2 sorption in Mg-MOF-74, Ni-MOF-74, and Co-MOF-74 range from approximately 30−27%, 35−31%, and 34−29% for 0.001 to 1.0 atm for the respective MOFs (see Supporting Information). Permanent electrostatic interactions contribute to about 32−27% for the same pressure range in Zn-MOF-74, which is higher than the percentages for polarization in this MOF. This indicates that electrostatic interactions are more important than polarization for H_2 sorption in Zn-MOF-74. It is also important to mention that, compared to the trend for the polarization contribution, the opposite trend can be observed for the van der Waals contribution for H_2 sorption in these MOFs—that is, Zn-MOF-74 > Mg-MOF-74 > Co-MOF-74 > Ni-MOF-74 (see Supporting Information).

E. Explanation of H_2 Sorption Trends. The observed H_2 sorption trends within the M-MOF-74 series can be explained, in part, by analyzing the calculated partial charges and polarizabilities for the metal ions in this work (see Methods section). Both the Ni^{2+} and Co^{2+} ions in their respective MOFs have high partial positive charges and polarizability values according to our electronic structure calculations; this can explain why Ni-MOF-74 and Co-MOF-74 have the highest initial H_2 Q_{st} values within the series. Since the sorption of H_2 onto the open-metal sites is dominated by polarization effects, it makes sense that having high partial charges and polarizability values for the metal ions in these MOFs will result in enhanced H_2−metal interactions.

Co^{2+} has a higher polarizability than Ni^{2+} (3.26440 vs 2.94650 Å^3) mainly due to the larger ionic radius of the former according to periodic trends. However, Ni-MOF-74 exhibits stronger H_2−metal interactions than Co-MOF-74 ostensibly due to the higher partial positive charge for the Ni^{2+} ions compared to the Co^{2+} ions (1.50150 vs 1.42010 e^-). Since higher partial charges on the metal greatly influence polarization interactions and increase the contributions from both stationary electrostatics and polarization, Ni-MOF-74 displays greater H_2−metal interactions because of this. The Ni^{2+} ion has a smaller ionic radius than Co^{2+}, which implies that Ni^{2+} has a greater tendency to give up its electrons (becoming more positively charged). This explains why the calculated partial charge for Ni^{2+} is greater than that for Co^{2+}.

When comparing the calculated partial charges for the metal ions within the four M-MOF-74 variants, it can be observed that the Mg^{2+} ion has the highest partial positive charge between the four metal ions, with a value of 1.67800 e^-. This is because the Mg^{2+} ion is the most electropositive species out of the four M^{2+} ions according to periodic trends. Despite having a very high partial charge, the calculated polarizability value for Mg^{2+} was found to be extremely low (0.00720 Å^3). This could be due to the fact that the very high tendency for the Mg^{2+} ion to give up its electrons would make it far less polarizable. This negligible polarizability value for Mg^{2+} certainly had an effect on the observed H_2−metal interaction in Mg-MOF-74 in comparison to Ni-MOF-74 and Co-MOF-74 according to the simulations performed in this work. Specifically, the initial H_2 Q_{st} value for Mg-MOF-74 is lower than that for Ni-MOF-74 and Co-MOF-74 due to the low polarizability of Mg^{2+}. Thus, even though the Mg^{2+} ion has the highest partial positive charge out of the four M^{2+} ions, the very small polarizability value for this ion causes Mg-MOF-74 to exhibit a weaker H_2−metal interaction compared to Ni-MOF-74 and Co-MOF-74. This highlights the interplay between the metal partial charge and polarizabilities in these MOFs in producing the energetics that are associated with the H_2−metal interaction.

The effects of the metal partial charge and polarizability values on capturing the H_2 sorption characteristics in these MOFs through GCMC simulation were further elucidated by performing control simulations in some of the M-MOF-74 analogues. To assess the importance of having a high polarizability value for the metal ion in Ni-MOF-74, control simulations were performed in this MOF by assigning all Ni^{2+} ions the value of the Mg^{2+} ion polarizability while keeping all other simulation parameters constant. It was observed that simulating H_2 sorption in Ni-MOF-74 using the aforementioned polarizability value for Ni^{2+} resulted in lower H_2 uptakes and Q_{st} values compared to the parent simulations in this MOF (see Supporting Information). This indicates that a high polarizability value for the Ni^{2+} ion is necessary to produce the

DOI: 10.1021/jp510253m
J. Phys. Chem. C 2015, 119, 1078−1090

strong H_2−metal interaction that is associated with this MOF in simulation.

Furthur, control simulations were performed in Mg-MOF-74 in which all Mg^{2+} ions were given the polarizability value that was calculated for Ni^{2+}. These simulations revealed that the MOF displayed a much sharper increase in H_2 uptake at low loading, which is accompanied by a higher initial Q_{st} value for H_2 (see Supporting Information). Thus, the H_2−metal interaction in Mg-MOF-74 is greater if a much higher polarizability value is used for Mg^{2+} rather than the original value that was calculated for this ion. This further suggests that the negligible polarizability value that was calculated for Mg^{2+} is responsible for the relatively lower H_2 Q_{st} values for Mg-MOF-74 compared to Ni-MOF-74 and Co-MOF-74 as observed experimentally. Note, even though Mg-MOF-74 exhibits a lower initial H_2 Q_{st} than Ni-MOF-74 and Co-MOF-74, this MOF has the highest initial Q_{st} value for CO_2 within the M-MOF-74 series according to experimental measurements.[12] It is expected that the sorption of CO_2 onto the metal ions in these MOFs is more dominated by electrostatic interactions (i.e., the partial charges on the metal), although polarization should also play a role in capturing the metal−sorbate interaction.

Note, it can be observed that, even though Mg-MOF-74 has a higher partial positive charge on the metal than in Ni-MOF-74, the calculated initial H_2 Q_{st} values for the former are still lower than those for the latter when both MOFs are given the same polarizability value for the metal ion. This suggests that the stronger H_2−metal interaction in Ni-MOF-74 compared to Mg-MOF-74 can also be attributed to steric effects within the crystal structures. When comparing the lattice parameters for the crystal structures between the four MOFs, the following trend can be observed for the a/b-axis distance: Zn-MOF-74 > Mg-MOF-74 > Co-MOF-74 > Ni-MOF-74 (see Supporting Infomation). It can be deduced that the initial H_2 Q_{st} value in the M-MOF-74 series increases as the length of the a/b dimension decreases. A shorter a/b-axis length implies smaller pore diameters within this series of MOFs.[15] Smaller pore sizes could provide for better synergistic interactions from a number of different moieties for the metal-sorbed H_2 molecules.

In addition, when comparing the size of the metal ions between Ni^{2+}, Co^{2+}, and Mg^{2+}, the Ni^{2+} ion has the smallest ionic radius, followed by Co^{2+} and Mg^{2+}; this is based on periodic trends for the atomic/ionic radius and is consistent with what was observed from DFT calculations on these ions in a previous study.[11] Smaller ionic radii usually correspond to shorter distances between the metal and the surrounding oxygen atoms in the structures of these MOFs. Indeed, inspection of the crystal structures for Ni-MOF-74, Co-MOF-74, and Mg-MOF-74 revealed that the M^{2+}−O distances are generally shorter for Ni-MOF-74 compared to those within the other two MOFs (Figure 4). Likewise, most of the M^{2+}−O distances are shorter in Co-MOF-74 relative to those in Mg-MOF-74. As the H_2 molecules approach the metal ions in these MOFs, smaller M^{2+}−O distances indicates that the framework oxygen atoms are able to interact more favorably with the H atom of the metal-sorbed H_2 molecule. Thus, with the oxygen atoms closer to the metal ions in these MOFs, the H_2−metal interaction increases due to enhanced cooperative effects between the H_2 molecules and the framework. As summarized in Table 3, most of the H−O distances are shorter for Ni-MOF-74 compared to those for the other two MOFs.

Although the Zn^{2+} ions have both a high partial charge in the Zn-MOF-74 environment (1.49240 e^-) and a reasonable magnitude polarizability value (1.98870 $Å^3$), Zn-MOF-74 sorbs the lowest H_2 uptake and has the weakest H_2−metal interaction within the series. Control simulations were performed in Zn-MOF-74 using the partial charges that were derived for the other M-MOF-74 analogues to gain insights into this issue. It was observed that the H_2 uptakes and Q_{st} values in Zn-MOF-74 were still the lowest between the four MOFs. Thus, it seems that the choice of the charge distribution plays a small role for simulations of H_2 sorption in Zn-MOF-74.

Further, the Zn^{2+} ion has the smallest ionic radius between the four metal ions according to periodic trends, thus implying that Zn-MOF-74 should have the shortest M^{2+}−O distances within the series. However, as observed in the crystal structure for Zn-MOF-74, this is not the case. This suggests that the weak H_2−metal interaction in Zn-MOF-74 (in comparison to the other M-MOF-74 analogues) is due to steric effects within the crystal structure of the MOF that is related to the geometry of the ZnO_5 cluster. Indeed, it was observed that, unlike in the other three M-MOF-74 analogues, the Zn^{2+} ions in Zn-MOF-74 do not form a representative square pyramidal MO_5 cluster in the structure, as one of the oxygen atoms from this cluster is projected outward into the accessible channels (Figure 4d). This outward shift by one of the oxygen atoms prevents the H_2 molecules from getting closer to the metal, thus explaining the weaker H_2−metal interaction. It is predicted that the ZnO_5 clusters have this particular arrangement in Zn-MOF-74 because the Zn^{2+} ions are attempting to form a tetrahedral coordination environment with the surrounding oxygen atoms, which it has preference for over a 5-connected or 6-connected coordination environment. However, due to the topology of the MOF, all Zn^{2+} ions are forced to be 5-connected in the material (or 6-connected in the as-synthesized structure).

F. Inelastic Neutron Scattering and Quantum Rotation Calculations. The INS spectrum for H_2 sorbed in all four MOFs at a loading of 0.50 H_2 molecules per metal (or 0.50 mol mol^{-1}) are shown in Figure 7. The spectra for Mg-MOF-74 and Ni-MOF-74 were collected at the cold neutron time-of-flight spectrometer FOCUS (at the Swiss neutron source SINQ of

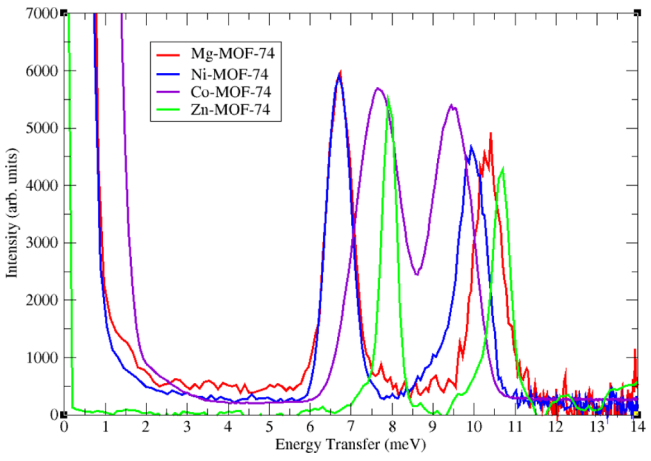

Figure 7. Inelastic neutron scattering (INS) spectra for H_2 in Mg-MOF-74 (red), Ni-MOF-74 (blue), Co-MOF-74 (violet), and Zn-MOF-74 (green) at a loading of 0.5 H_2 per metal. The spectra for Mg-MOF-74 and Ni-MOF-74 were collected on the FOCUS spectrometer at SINQ. The spectrum for Co-MOF-74 was collected on the TOFTOF spectrometer at the FRM-II. The spectrum for Zn-MOF-74 was collected on the QENS spectrometer at IPNS. Note, the intensities of the spectra were scaled relative to each other.

DOI: 10.1021/jp510253m
J. Phys. Chem. C 2015, 119, 1078−1090

the Paul Scherrer Institute, Villigen, Switzerland).[15] The INS spectrum for Co-MOF-74 was collected at TOFTOF (at the FRM-II, Munich, Germany), while the spectrum for Zn-MOF-74 was collected at the QENS spectrometer (at the neutron source IPNS of Argonne National Laboratory). The INS spectra for Mg-MOF-74, Ni-MOF-74, and Co-MOF-74 were collected at a temperature of 1.5 K, while the spectra for Zn-MOF-74 were collected at 10 K. Although the spectrum at 0.50 H_2/Zn is shown in Figure 7 for Zn-MOF-74, the spectra at other loadings for this MOF are provided in the Supporting Information.

The transitions that appear in the INS spectra for H_2 in MOFs are mainly due to the rotational excitations of the H_2 molecules in the MOF. In the absence of a barrier to rotation, a H_2 molecule rotates freely with energy levels that are characteristic of a rigid rotor. However, in the presence of an external field, such as a MOF sorption site, a rotational barrier is imparted on the H_2 molecule. As a result, the energies for each j level are split since the $(2j + 1)$ degeneracy is lifted. In the INS spectra for H_2 in MOFs, rotational tunnelling transitions that occur at low energies correspond to high barriers to rotation and strong interactions with the MOF.

A pair of peaks can be observed in the INS spectrum for all four MOFs (Mg-MOF-74: 6.7 and 10.2 meV; Ni-MOF-74: 6.7 and 9.9 meV; Co-MOF-74: 7.6 and 9.4 meV; Zn-MOF-74: 7.9 and 10.7 meV).[15] Note, the INS spectrum shown herein for Mg-MOF-74 and Zn-MOF-74 are similar to those reported in refs 16 and 20, respectively. As established previously, both of these peaks in all four MOFs correspond to the sorption of H_2 onto the metal centers in the respective MOFs.[15,16,20,31] Although the INS spectrum for H_2 in all four M-MOF-74 variants appear similar to each another, some differences in the observed rotational transitions can be observed.

The calculated two-dimensional quantum rotational levels for a H_2 molecule sorbed about the M^{2+} ion in all four MOFs are shown in Table 4. Only the rotational levels for the two lowest transitions are shown since these levels can be directly compared to the transitions for the two noticeable peaks in the INS spectra for the given energy range. For each MOF, the calculated rotational levels are based on the optimized H_2 molecule positions that were determined using simulated annealing. Furthermore, the rotational levels reported herein were calculated using the classical potential energy function employed this work. As described in the Methods, the form of the potential is simple as it is sum of the Lennard-Jones potential, the electrostatic potential energy as calculated via Ewald summation, and the many-body polarization energy as calculated using a Thole–Applequist type model. This is in contrast to what was executed in previous work,[31,61,62] most notably in ref 31, where the rotational potential was calculated using periodic DFT calculations for Zn-MOF-74.

Table 4. Calculated Two-Dimensional Quantum Rotational Levels for the Two Lowest Transitions for a H_2 Molecule Sorbed onto the M^{2+} Ion in the M-MOF-74 Series (M = Mg, Ni, Co, Zn)[a]

transition	Mg-MOF-74	Ni-MOF-74	Co-MOF-74	Zn-MOF-74
1	7.17	6.26	7.46	8.37
2	9.95	9.84	9.71	11.45

[a]Relative energies are given in meV.

The calculations performed herein revealed noticeable differences in the transitions for the H_2–metal interaction for all four MOFs. Our calculations revealed that the M^{2+}–H_2 interaction in Ni-MOF-74 has the lowest energy for the lowest transition within the M-MOF-74 series, with a calculated rotational level of 6.26 meV. This was to be expected since, according to our calculations, the H_2 molecule is sorbed closer to the metal in Ni-MOF-74 relative to the other three variants; this indicates stronger H_2–metal interactions. The calculated energy level for the lowest transition is slightly lower than the observed 6.7 meV peak in the INS spectra for Ni-MOF-74, but it is still in good agreement nonetheless. The second transition for the H_2–metal interaction in Ni-MOF-74 was calculated to be 9.84 meV, which is in excellent agreement with the 9.9 meV peak for this MOF.

Interestingly, the lowest energy peak for Co-MOF-74 is found at higher energies than the corresponding peak in Mg-MOF-74 (7.6 vs 6.7 meV) even though the former exhibits a stronger H_2–metal interaction. This observation is supported by our quantum rotation calculations for the H_2–metal in the two MOFs, as the calculated rotational levels for the first transition were 7.46 and 7.17 meV for Co-MOF-74 and Mg-MOF-74, respectively. These levels are in good agreement with the corresponding experimental values. It is also interesting that the lowest energy peak for Mg-MOF-74 is the same as that for Ni-MOF-74 (6.7 meV). Our calculated rotational level for the second transition for the H_2–metal interaction in Mg-MOF-74 (9.95 meV) is slightly lower than the transition energy for the second peak in this MOF (10.2 meV), but it is still within the vicinity of experiment. In addition, consistent with experiment, the calculated rotational level for the second transition in Mg-MOF-74 (9.95 meV) is higher than that for the matching transition in Ni-MOF-74 (9.84 meV). Note, the rotational levels calculated herein for the H_2–metal interaction in Mg-MOF-74 is slightly different from what was calculated for this interaction in our previous work on this MOF (7.08 and 10.62 meV).[43] This is because our recent study utilized a H_2–metal distance of 2.60 Å, whereas a distance of 2.55 Å was used for the calculations in the present work. This indicates that the calculated rotational levels are highly dependent on the H_2 molecule position within the MOF system cell.

As observed in Figure 7, the second transition for Co-MOF-74 is found at lower energies when comparing to the energies for the corresponding transitions between the three MOFs; this is also in accord with our calculations (Table 4). We suspect that minor differences in the orientations of the neighboring oxygen atoms as well as the geometry of the sorbed H_2 molecule about the M^{2+} ion between the MOFs are responsible for these observations (Figure 4). Nevertheless, the observed and calculated transitions for the H_2–metal interaction in Mg-MOF-74, Ni-MOF-74, and Co-MOF-74 are similar between each other, which suggests that the rotational potential for this interaction within this series of MOFs is nearly independent of the nature of the metal.

As revealed in the INS spectra, Zn-MOF-74 has the highest energies for the two transitions for the H_2–metal interaction within the series. This was convincingly supported by our calculations, as the rotational energy levels for the first two transitions were calculated to be 8.37 and 11.45 meV, respectively; these are higher than the corresponding transitions that were calculated for the other three MOFs. Since Zn-MOF-74 has the lowest H_2 Q_{st} and the longest H_2–metal distance within the series, it makes sense that the

DOI: 10.1021/jp510253m
J. Phys. Chem. C 2015, 119, 1078–1090

rotational tunnelling transitions for this MOF are found at higher energies compared to those for the other members. The aforementioned levels for Zn-MOF-74 are in good agreement with the two transitions that occur in the INS spectra for the MOF as shown herein (7.9 and 10.7 meV). Note, the rotational levels for the two lowest transitions calculated for Zn-MOF-74 in this work is in very good agreement with the peaks that appear in the INS spectra reported in ref 20 for this MOF (8.3 and 11.3 meV), where the spectra were collected using a different spectrometer and MOF sample than what were used in this work.

The rotational levels that were calculated for the corresponding transitions using DFT methods for Zn-MOF-74 as performed in ref 31 were only in modest agreement with experiment (10.6 and 14.0 meV). This suggests that DFT methods cannot predict the rotational energy levels for H_2 in a M-MOF-74 system (and other MOFs, in general) very well even though such methods can correctly calculate the binding energy for the metal−sorbate interaction. Indeed, obtaining accurate rotational transitions using DFT methods is difficult to accomplish. In contrast, the rotational energy levels that were calculated for the H_2−metal interaction in all four members of the M-MOF-74 series using our analytical potential energy function in this work were in very good agreement with experiment. Note, the ability to predict and explain INS data for H_2 in MOFs using a classical potential energy function is an important scientific aspect presented in this work. DFT methods usually have difficulty with this task. Using spectroscopy to interrogate the nature of sorption mechanisms in MOFs is critically aided by such modeling that simultaneously serves to validate the fidelity of the associated modeling methodology via its predictive and explanatory value.

IV. CONCLUSION

In summary, we simulated H_2 sorption in Mg-MOF-74, Ni-MOF-74, Co-MOF-74, and Zn-MOF-74 in order to elucidate the observed experimental H_2 sorption trends within the M-MOF-74 series. Our simulated H_2 sorption isotherms and Q_{st} values for all four MOFs were in very good agreement with the corresponding experimental data. Such agreement between the experimental and theoretical H_2 sorption data within the M-MOF-74 series was achieved with the implementation of classical polarization in simulation. Indeed, we provided a suitable model for the accurate simulations of H_2 sorption within the M-MOF-74 series.

Experimental studies have shown the following trend for the H_2−metal interaction in the M-MOF-74 series: Ni-MOF-74 > Co-MOF-74 > Mg-MOF-74 > Zn-MOF-74; this trend was surprisingly reproduced in simulation using our predictive modeling. In general, it was observed that the greater the contribution from polarization, the stronger the H_2−metal interaction within this series of MOFs. As observed through electronic structure calculations in all four MOFs, the differences in the charge distribution and metal polarizability between the MOFs explained some of the observed H_2 sorption trends within this series. The H_2 sorption trends were also explained by steric effects within the crystal structures of the MOFs as notable differences were observed in the M^{2+}−O distances for each MOF. This conclusion was further supported by control simulations in two of the members of the M-MOF-74 series. In addition, we observed that Zn-MOF-74 has the lowest H_2 uptake and Q_{st} within the series due to an unusual arrangement of one of the oxygen atoms within the ZnO_5 clusters that prevented the H_2 molecules from getting closer to the metal.

In general, the calculated rotational levels reported in this work for the H_2−metal interaction in all M-MOF-74 analogues are in good agreement with the corresponding INS spectra for the MOFs. We have shown that the rotational transitions for a H_2 molecule sorbed about the metal ion in this series of MOFs can accurately be predicted using a classical potential energy function. Further, the results from the INS studies and the quantum rotation calculations performed herein for all four MOFs suggest that the rotational potential for the H_2−metal interaction in these MOFs is nearly independent of the identity of the metal. Indeed, no specific trend was observed for the rotational transitions for the H_2−metal interactions in these MOFs based on experimental INS data and our quantum rotation calculations. For instance, even though Ni-MOF-74 displays a higher initial H_2 Q_{st} than Mg-MOF-74, INS studies revealed that the first transition for the H_2−metal interaction in these two MOFs occur at the same transition energy in the resultant spectra. Thus, this implies that the rotational potential for the H_2−metal interaction in the M-MOF-74 series is more governed by the oxygen atoms that surround the metal ions.

Although it was observed that the trend in the H_2−metal interaction in the M-MOF-74 series is Ni-MOF-74 > Co-MOF-74 > Mg-MOF-74 > Zn-MOF-74, different sorption trends can be observed for other sorbates.[12,63] For instance, experimental studies on CO_2 sorption in the M-MOF-74 series revealed the following trends for the initial CO_2 Q_{st} values, and hence the CO_2−metal interaction: Mg-MOF-74 > Ni-MOF-74 > Co-MOF-74 > Zn-MOF-74.[12] When comparing the partial charges for the metal ions between Mg-MOF-74, Ni-MOF-74, and Co-MOF-74, the Mg^{2+} ion has the highest partial positive charge according to our calculations, followed by Ni^{2+} and then Co^{2+}. It is expected that the higher the partial charge on the metal (between Mg-MOF-74, Ni-MOF-74, and Co-MOF-74), the greater the CO_2−metal interaction because CO_2 sorption in these MOFs should be more dominated by permanent electrostatic interactions, in contrast to polarization interactions in the case of H_2 sorption, due to the high partial positive charge on the metal and the high molecular quadrupole of the CO_2 molecule. Zn-MOF-74 should have the weakest CO_2−metal interaction within the series due to same steric reasons as described above. It is planned to investigate and confirm these trends in future theoretical studies within the M-MOF-74 series.

■ ASSOCIATED CONTENT

Supporting Information

Details of grand canonical Monte Carlo methods, many-body polarization overview, tables of properties, details of quantum rotation calculations, and additional H_2 sorption results. This material is available free of charge via the Internet at http://pubs.acs.org.

■ AUTHOR INFORMATION

Corresponding Author

*(B.S.) E-mail: bspace@mail.usf.edu.

Notes

The authors declare no competing financial interest.

DOI: 10.1021/jp510253m
J. Phys. Chem. C 2015, 119, 1078−1090

■ ACKNOWLEDGMENTS

B.S. acknowledges the National Science Foundation (Award No. CHE-1152362), the computational resources that were made available by a XSEDE Grant (No. TG-DMR090028), and the use of the services provided by Research Computing at the University of South Florida. This publication is also based on work supported by Award No. FIC/2010/06, made by the King Abdullah University of Science and Technology (KAUST). The authors also thank the Space Foundation (Basic and Applied Research) for partial support.

■ REFERENCES

(1) Collins, D. J.; Zhou, H.-C. Hydrogen storage in metal−organic frameworks. *J. Mater. Chem.* **2007**, *17*, 3154−3160.
(2) Zhao, D.; Yuan, D.; Zhou, H.-C. The current status of hydrogen storage in metal−organic frameworks. *Energy Environ. Sci.* **2008**, *1*, 222−235.
(3) Suh, M. P.; Park, H. J.; Prasad, T. K.; Lim, D.-W. Hydrogen Storage in Metal−Organic Frameworks. *Chem. Rev.* **2012**, *112*, 782−835.
(4) Bhatia, S. K.; Myers, A. L. Optimum Conditions for Adsorptive Storage. *Langmuir* **2006**, *22*, 1688−1700.
(5) Ma, S. Gas adsorption applications of porous metal−organic frameworks. *Pure Appl. Chem.* **2009**, *81*, 2235−2251.
(6) Rosi, N. L.; Kim, J.; Eddaoudi, M.; Chen, B.; O'Keeffe, M.; Yaghi, O. M. Rod Packings and Metal−Organic Frameworks Constructed from Rod-Shaped Secondary Building Units. *J. Am. Chem. Soc.* **2005**, *127*, 1504−1518, PMID: 15686384.
(7) Dietzel, P. D. C.; Morita, Y.; Blom, R.; Fjellvåg, H. An In Situ High-Temperature Single-Crystal Investigation of a Dehydrated Metal−Organic Framework Compound and Field-Induced Magnetization of One-Dimensional Metal−Oxygen Chains. *Angew. Chem., Int. Ed.* **2005**, *44*, 6354−6358.
(8) Rowsell, J. L. C.; Yaghi, O. M. Effects of Functionalization, Catenation, and Variation of the Metal Oxide and Organic Linking Units on the Low-Pressure Hydrogen Adsorption Properties of Metal−Organic Frameworks. *J. Am. Chem. Soc.* **2006**, *128*, 1304−1315, PMID: 16433549.
(9) Dietzel, P. D.; Panella, B.; Hirscher, M.; Blom, R.; Fjellvåg, H. Hydrogen adsorption in a nickel based coordination polymer with open metal sites in the cylindrical cavities of the desolvated framework. *Chem. Commun.* **2006**, 959−961.
(10) Dietzel, P. D.; Johnsen, R. E.; Blom, R.; Fjellvåg, H. Structural Changes and Coordinatively Unsaturated Metal Atoms on Dehydration of Honeycomb Analogous Microporous Metal−Organic Frameworks. *Chemistry: A European Journal* **2008**, *14*, 2389−2397.
(11) Zhou, W.; Wu, H.; Yildirim, T. Enhanced H_2 Adsorption in Isostructural Metal−Organic Frameworks with Open Metal Sites: Strong Dependence of the Binding Strength on Metal Ions. *J. Am. Chem. Soc.* **2008**, *130*, 15268−15269.
(12) Caskey, S. R.; Wong-Foy, A. G.; Matzger, A. J. Dramatic Tuning of Carbon Dioxide Uptake via Metal Substitution in a Coordination Polymer with Cylindrical Pores. *J. Am. Chem. Soc.* **2008**, *130*, 10870−10871, PMID: 18661979.
(13) Britt, D.; Furukawa, H.; Wang, B.; Glover, T. G.; Yaghi, O. M. Highly efficient separation of carbon dioxide by a metal−organic framework replete with open metal sites. *Proc. Natl. Acad. Sci. U.S.A.* **2009**, *106*, 20637−20640.
(14) Dietzel, P. D.; Besikiotis, V.; Blom, R. Application of metal−organic frameworks with coordinatively unsaturated metal sites in storage and separation of methane and carbon dioxide. *J. Mater. Chem.* **2009**, *19*, 7362−7370.
(15) Dietzel, P. D. C.; Georgiev, P. A.; Eckert, J.; Blom, R.; Strassle, T.; Unruh, T. Interaction of hydrogen with accessible metal sites in the metal-organic frameworks M_2(dhtp) (CPO-27-M; M = Ni, Co, Mg). *Chem. Commun.* **2010**, *46*, 4962−4964.
(16) Sumida, K.; Brown, C. M.; Herm, Z. R.; Chavan, S.; Bordiga, S.; Long, J. R. Hydrogen storage properties and neutron scattering studies of Mg_2(dobdc)−a metal−organic framework with open Mg^{2+} adsorption sites. *Chem. Commun.* **2011**, *47*, 1157−1159.
(17) Herm, Z. R.; Swisher, J. A.; Smit, B.; Krishna, R.; Long, J. R. Metal−Organic Frameworks as Adsorbents for Hydrogen Purification and Precombustion Carbon Dioxide Capture. *J. Am. Chem. Soc.* **2011**, *133*, 5664−5667.
(18) Marcz, M.; Johnsen, R. E.; Dietzel, P. D.; Fjellvag, H. The iron member of the CPO-27 coordination polymer series: Synthesis, characterization, and intriguing redox properties. *Microporous Mesoporous Mater.* **2012**, *157*, 62−74.
(19) Vitillo, J. G.; Regli, L.; Chavan, S.; Ricchiardi, G.; Spoto, G.; Dietzel, P. D. C.; Bordiga, S.; Zecchina, A. Role of Exposed Metal Sites in Hydrogen Storage in MOFs. *J. Am. Chem. Soc.* **2008**, *130*, 8386−8396.
(20) Liu, Y.; Kabbour, H.; Brown, C. M.; Neumann, D. A.; Ahn, C. C. Increasing the Density of Adsorbed Hydrogen with Coordinatively Unsaturated Metal Centers in Metal−Organic Frameworks. *Langmuir* **2008**, *24*, 4772−4777.
(21) Valenzano, L.; Civalleri, B.; Chavan, S.; Palomino, G. T.; Areán, C. O.; Bordiga, S. Computational and Experimental Studies on the Adsorption of CO, N_2, and CO_2 on Mg-MOF-74. *J. Phys. Chem. C* **2010**, *114*, 11185−11191.
(22) Valenzano, L.; Civalleri, B.; Sillar, K.; Sauer, J. Heats of Adsorption of CO and CO_2 in Metal−Organic Frameworks: Quantum Mechanical Study of CPO-27-M (M = Mg, Ni, Zn). *J. Phys. Chem. C* **2011**, *115*, 21777−21784.
(23) Dzubak, A. L.; Lin, L.-C.; Kim, J.; Swisher, J. A.; Poloni, R.; Maximoff, S. N.; Smit, B.; Gagliardi, L. Ab initio carbon capture in open-site metal−organic frameworks. *Nat. Chem.* **2012**, *4*, 810−816.
(24) Lin, L.-C.; Lee, K.; Gagliardi, L.; Neaton, J. B.; Smit, B. Force-Field Development from Electronic Structure Calculations with Periodic Boundary Conditions: Applications to Gaseous Adsorption and Transport in Metal−Organic Frameworks. *J. Chem. Theory Comput.* **2014**, *10*, 1477−1488.
(25) Sillar, K.; Sauer, J. Ab Initio Prediction of Adsorption Isotherms for Small Molecules in Metal−Organic Frameworks: The Effect of Lateral Interactions for Methane/CPO-27-Mg. *J. Am. Chem. Soc.* **2012**, *134*, 18354−18365.
(26) Bloch, E. D.; et al. Reversible CO Binding Enables Tunable CO/H_2 and CO/N_2 Separations in Metal−Organic Frameworks with Exposed Divalent Metal Cations. *J. Am. Chem. Soc.* **2014**, *136*, 10752−10761.
(27) Forrest, K. A.; Pham, T.; McLaughlin, K.; Belof, J. L.; Stern, A. C.; Zaworotko, M. J.; Space, B. Simulation of the Mechanism of Gas Sorption in a Metal−Organic Framework with Open Metal Sites: Molecular Hydrogen in PCN-61. *J. Phys. Chem. C* **2012**, *116*, 15538−15549.
(28) Pham, T.; Forrest, K. A.; Nugent, P.; Belmabkhout, Y.; Luebke, R.; Eddaoudi, M.; Zaworotko, M. J.; Space, B. Understanding Hydrogen Sorption in a Metal−Organic Framework with Open-Metal Sites and Amide Functional Groups. *J. Phys. Chem. C* **2013**, *117*, 9340−9354.
(29) Pham, T.; Forrest, K. A.; Hogan, A.; McLaughlin, K.; Belof, J. L.; Eckert, J.; Space, B. Simulations of Hydrogen Sorption in *rht*-MOF-1: Identifying the Binding Sites Through Explicit Polarization and Quantum Rotation Calculations. *J. Mater. Chem. A* **2014**, *2*, 2088−2100.
(30) Pham, T.; Forrest, K. A.; Eckert, J.; Georgiev, P. A.; Mullen, A.; Luebke, R.; Cairns, A. J.; Belmabkhout, Y.; Eubank, J. F.; McLaughlin, K.; Lohstroh, W.; Eddaoudi, M.; Space, B. Investigating the Gas Sorption Mechanism in an *rht*-Metal−Organic Framework through Computational Studies. *J. Phys. Chem. C* **2014**, *118*, 439−456.
(31) Kong, L.; Román-Pérez, G.; Soler, J. M.; Langreth, D. C. Energetics and Dynamics of H_2 Adsorbed in a Nanoporous Material at Low Temperature. *Phys. Rev. Lett.* **2009**, *103*, 096103.
(32) Matanović, I.; Belof, J. L.; Space, B.; Sillar, K.; Sauer, J.; Eckert, J.; Bačić, Z. Hydrogen adsorbed in a metal organic framework-5:

DOI: 10.1021/jp510253m
J. Phys. Chem. C 2015, 119, 1078−1090

Coupled translation-rotation eigenstates from quantum five-dimensional calculations. *J. Chem. Phys.* **2012**, *137*, 014701.
(33) Nugent, P.; Pham, T.; McLaughlin, K.; Georgiev, P. A.; Lohstroh, W.; Embs, J. P.; Zaworotko, M. J.; Space, B.; Eckert, J. Dramatic effect of pore size reduction on the dynamics of hydrogen adsorbed in metal−organic materials. *J. Mater. Chem. A* **2014**, *2*, 13884−13891.
(34) Pham, T.; Forrest, K. A.; Georgiev, P. A.; Lohstroh, W.; Xue, D.-X.; Hogan, A.; Eddaoudi, M.; Space, B.; Eckert, J. A high rotational barrier for physisorbed hydrogen in an fcu-metal−organic framework. *Chem. Commun.* **2014**, *50*, 14109−14112.
(35) Metropolis, N.; Rosenbluth, A. W.; Rosenbluth, M. N.; Teller, A. H.; Teller, E. Equation of state calculations by fast computing machines. *Phys. Lett. B* **1953**, *21*, 1087−1092.
(36) Ewald, P. P. Die Berechnung optischer und elektrostatischer Gitterpotentiale. *Ann. Phys.* **1921**, *369*, 253−287.
(37) Applequist, J.; Carl, J. R.; Fung, K.-K. Atom dipole interaction model for molecular polarizability. Application to polyatomic molecules and determination of atom polarizabilities. *J. Am. Chem. Soc.* **1972**, *94*, 2952−2960.
(38) Thole, B. Molecular polarizabilities calculated with a modified dipole interaction. *Chem. Phys.* **1981**, *59*, 341−350.
(39) Bode, K. A.; Applequist, J. A New Optimization of Atom Polarizabilities in Halomethanes, Aldehydes, Ketones, and Amides by Way of the Atom Dipole Interaction Model. *J. Phys. Chem.* **1996**, *100*, 17820−17824.
(40) McLaughlin, K.; Cioce, C. R.; Pham, T.; Belof, J. L.; Space, B. Efficient calculation of many-body induced electrostatics in molecular systems. *J. Chem. Phys.* **2013**, *139*, 184112.
(41) Feynman, R. P.; Hibbs, A. R. *Quantum Mechanics and Path Integrals*; McGraw-Hill: New York, 1965; pp 281.
(42) Belof, J. L.; Stern, A. C.; Space, B. An Accurate and Transferable Intermolecular Diatomic Hydrogen Potential for Condensed Phase Simulation. *J. Chem. Theory Comput.* **2008**, *4*, 1332−1337.
(43) Pham, T.; Forrest, K. A.; McLaughlin, K.; Eckert, J.; Space, B. Capturing the H_2−Metal Interaction in Mg-MOF-74 Using Classical Polarization. *J. Phys. Chem. C* **2014**, *118*, 22683−22690.
(44) Rappé, A. K.; Casewit, C. J.; Colwell, K. S.; Goddard, W. A.; Skiff, W. M. UFF, a full periodic table force field for molecular mechanics and molecular dynamics simulations. *J. Am. Chem. Soc.* **1992**, *114*, 10024−10035.
(45) Belof, J. L.; Stern, A. C.; Space, B. A Predictive Model of Hydrogen Sorption for Metal−Organic Materials. *J. Phys. Chem. C* **2009**, *113*, 9316−9320.
(46) van Duijnen, P. T.; Swart, M. Molecular and Atomic Polarizabilities: Thole's Model Revisited. *J. Phys. Chem. A* **1998**, *102*, 2399−2407.
(47) Belof, J. L.; Stern, A. C.; Eddaoudi, M.; Space, B. On the Mechanism of Hydrogen Storage in a Metal−Organic Framework Material. *J. Am. Chem. Soc.* **2007**, *129*, 15202−15210, PMID: 17999501.
(48) Cirera, J.; Sung, J. C.; Howland, P. B.; Paesani, F. The effects of electronic polarization on water adsorption in metal−organic frameworks: H_2O in MIL-53(Cr). *J. Chem. Phys.* **2012**, *137*, 054704.
(49) Forrest, K. A.; Pham, T.; McLaughlin, K.; Hogan, A.; Space, B. Insights into an intriguing gas sorption mechanism in a polar metal−organic framework with open-metal sites and narrow channels. *Chem. Commun.* **2014**, *50*, 7283−7286.
(50) Shao, Y.; et al. Advances in methods and algorithms in a modern quantum chemistry program package. *Phys. Chem. Chem. Phys.* **2006**, *8*, 3172−3191.
(51) Belof, J. L.; Space, B. *Massively Parallel Monte Carlo (MPMC)*. Available on Google Code, 2012, https://code.google.com/p/mpmc/.
(52) Kirkpatrick, S.; Gelatt, C. D.; Vecchi, M. P. Optimization by simmulated annealing. *Science* **1983**, *220*, 671−680.
(53) Buch, V. Path integral simulations of mixed para-D_2 and ortho-D_2 clusters: The orientational effects. *J. Chem. Phys.* **1994**, *100*, 7610−7629.
(54) Darkrim, F.; Levesque, D. Monte Carlo simulations of hydrogen adsorption in single-walled carbon nanotubes. *J. Chem. Phys.* **1998**, *109*, 4981−4984.
(55) Mankoo, P. K.; Keyes, T. Classical Molecular Electrostatics: Recognition of Ligands in Proteins and the Vibrational Stark Effect. *J. Phys. Chem. B* **2006**, *110*, 25074−25079, PMID: 17149932.
(56) Kumar, R.; Keyes, T. Classical Simulations with the POLIR Potential Describe the Vibrational Spectroscopy and Energetics of Hydration: Divalent Cations, from Solvation to Coordination Complex. *J. Am. Chem. Soc.* **2011**, *133*, 9441−9450.
(57) Eckert, J.; Kubas, G.; Hall, J.; Hay, P.; Boyle, C. Molecular hydrogen complexes. VI: The barrier to rotation of η^2-H_2 in $M(CO)_3(PR_3)_2(\eta^2\text{-}H_2)$(M = W, Mo; R = Cy, *i*-Pr): Inelastic Neutron Scattering, Theoretic al, and Molecular Mechanics Studies. *J. Am. Chem. Soc.* **1990**, *112*, 2324−2332.
(58) Kubas, G. J. *Metal Dihydrogen and σ-Bond Complexes: Structure, Theory, and Reactivity*; Kluwer Academic Publishers: New York, 2001.
(59) Brown, C. M.; Ramirez-Cuesta, A. J.; Her, J.-H.; Wheatley, P. S.; Morris, R. E. Structure and spectroscopy of hydrogen adsorbed in a nickel metal−organic framework. *Chem. Phys.* **2013**, *427*, 3−8.
(60) Kapelewski, M. T.; Geier, S. J.; Hudson, M. R.; Stck, D.; Mason, J. A.; Nelson, J. N.; Xiao, D. J.; Hulvey, Z.; Gilmour, E.; FitzGerald, S. A.; Head-Gordon, M.; Brown, C. M.; Long, J. R. M_2(*m*-dobdc) (M = Mg, Mn, Fe, Co, Ni) Metal−Organic Frameworks Exhibiting Increased Charge Density and Enhanced H_2 Binding at the Open Metal Sites. *J. Am. Chem. Soc.* **2014**, *136*, 12119−12129, PMID: 25130365.
(61) Kong, L.; Chabal, Y. J.; Langreth, D. C. First-principles approach to rotational-vibrational frequencies and infrared intensity for H_2 adsorbed in nanoporous materials. *Phys. Rev. B* **2011**, *83*, 121402.
(62) Brown, C. M.; Liu, Y.; Yildirim, T.; Peterson, V. K.; Kepert, C. J. Hydrogen adsorption in HKUST-1: a combined inelastic neutron scattering and first-principles study. *Nanotechnology* **2009**, *20*, 204025.
(63) Perry, J. J.; Teich-McGoldrick, S. L.; Meek, S. T.; Greathouse, J. A.; Haranczyk, M.; Allendorf, M. D. Noble Gas Adsorption in Metal−Organic Frameworks Containing Open Metal Sites. *J. Phys. Chem. C* **2014**, *118*, 11685−11698.

DOI: 10.1021/jp510253m
J. Phys. Chem. C 2015, 119, 1078−1090